A Journal of the Gesellschaft Deutscher Chemiker

Angewandte International Edition GDCh Chemie

www.angewandte.org

Accepted Article

Title: Silica Jar-with-Lid as Chemo-Enzymatic Nano-Compartment for Enantioselective Synthesis inside Living Cells

Authors: Seonock Kim, Nitee Kumari, Jongwon Lim, Sateesh Dubbu, Amit Kumar, and In Su Lee

To be cited as: *Angew. Chem. Int. Ed.* 10.1002/anie.202103165

Link to VoR: https://doi.org/10.1002/anie.202103165

WILEY-VCH

10.1002/anie.202103165

WILEY-VCH

COMMUNICATION

Silica Jar-with-Lid as Chemo-Enzymatic Nano-Compartment for Enantioselective Synthesis inside Living Cells

Seonock Kim,[a] Nitee Kumari,[a] Jongwon Lim,[a] Sateesh Dubbu,[a] Amit Kumar*[a] and In Su Lee*[a,b]

Abstract: Nanodevices, harvesting the power of synthetic catalysts and enzymes to perform enantioselective synthesis inside cell, have never been reported. Here, we synthesized round bottom *jar-like* silica nanostructures (**SiJAR**s) with a chemo-responsive metal-silicate *lid*. This was isolated as an intermediate structure during highly controlled solid-state nanocrystal-conversion at the arc-section of silica shell. Different catalytic noble metals (Pt, Pd, Ru) were selectively modified on the *lid*-section through galvanic reactions. And, *lid* aperture-opening was regulated by mild acidic conditions or intracellular environment which accommodated the metal nanocrystals and enzymes, and in turn created an open-mouth nanoreactor. Distinct from the free enzymes, **SiJAR**s performed asymmetric aldol reactions with high activity and enantioselectivity (yield >99%, ee = 95%) and also functioned as the artificial catalytic organelles inside living cells. This work bridges the enormous potential of sophisticated nanocrystal-conversion chemistry and advanced platforms for new-to-nature catalysis.

Evolutionary compartmentalization is the key structural feature of various organelles and cells to accommodate specific enzymes and cofactors, which effortlessly drive life-sustaining multistep biochemical cascades.[1] artificial organelle-like nanoreactors harnessing high activity of synthetic catalysts along with inherent handedness of enzymes, can result diversified platforms for bioorthogonal synthesis.[2,3] These chemo-enzymatic systems can asymmetrically synthesize chiral enantiomeric bioactive molecules,[4] possessing distinct pharmacological and toxicological systemic responses and in turn leading to advanced bioimaging, therapeutic and biotechnological applications.[5] Variety of nature-inspired hollow nanostructures, which consist of silica/silicate[4b,c,6] and polymers/micelles[3a,7] confining catalytic nanocrystals (NCs), enzymes or both, have demonstrated improved catalysis that are mostly limited to abiotic conditions.[8] Microemulsion-, sacrificial template-, and one-pot entrapment-based methods for pre-encapsulation of bio/nano-catalyts inside a confining nano-housing, often involve difficult to control multiple synthetic steps, harsh conditions, biphasic non-aqueous solvents and complex reagents.[9] Major challenge to design nanoreactors for intracellular application is to reliably co-localize and maintain the reactive surfaces of catalytic NCs along with the protection of enzymes from de-activation.[4,10] In this regard, silica nanostructures are highly appealing for wide range of catalytic and biomedical applications owing to their chemical inertness, high stability, biocompatibility and synthetic flexibility.[11] Previously, we developed solid-state conversion strategy for reversible hollowing of silica-coated manganese oxide ($MnO@SiO_2$)[12] and the post-synthetic modification of the hollow silica interiors with catalytic noble metals.[13] However, these microporous closed shells restrict the entry and co-localization of catalytic NCs and large-size biomolecules. To realize the intended open-mouthed shell-morphology for the construction of chemo-enzymatic nano-compartment,[14] it's crucial to modify the composition of selected shell-arc-section. We thought to utilize a yolk-like MnO NC as a metal-nano-reservoir inside hollow silica (*h*-SiO_2), for intrashell directional supply of Mn^{2+} ions localized only to the touching small arc inside *h*-SiO_2, while restricting its transformation to the thermodynamically stable structure having homogeneous phase.[12,15] Such spatiotemporally controlled thermal conversion chemistry would modify the composition of *h*-SiO_2 within the few-nm proximal in-contact section which can be selectively opened or chemically modified for further catalytic customization (Figure 1). Here, we report the synthesis of round bottom *jar-like* glass-phase nanostructure (designated as **SiJAR**) installed with a $MnSiO_3$-based chemically responsive *lid* of controllable section area. Owing to the segmented composition of the **SiJAR**, different catalytic noble metals (Pt, Pd, Ru) were selectively modified on the *lid*-section through galvanic replacement reaction.[13,16] Subsequently, lid aperture-opening was regulated by mild acidic conditions or intracellular environment, creating a wide-passage into the shell while shifting the residual metal NCs inwards. This strategy created customizable open-mouth hollow nanoreactors [**M**(M = Pt, Pd, Ru)**-SiJAR**s] which further facilitated the entry and encapsulation of large size enzymes inside the semi-confined concave structure (Figure 1).[17] Distinct from the promiscuous free enzymes, these nanoreactors performed asymmetric aldol reactions with high enantioselectivity (*ca*. 95% ee) via an enzyme-metal co-operative transition state stabilization, while protecting the NCs and enzymes within an open mouth silica-compartment and even functioned inside living cells like artificial catalytic organelles.

First, we installed MnO nanocube (edge = 20 ± 5 nm) inside *h*-SiO_2 [shell thickness = 10 ± 4nm, outer diameter = 108 ± 3 nm] by sequential silica encapsulation and hydrolytic hollowing steps. The resulting yolk-shell structure (MnO@*h*-SiO_2) possessed a dynamic configuration, where MnO NC docked to a selected few-nm interior arc-section of *h*-SiO_2 to induce an interfacial solid-state phase mixing process (Figure 1). The annealing of MnO@*h*-SiO_2 at temperature (T_{ann}) 800 °C under Ar + 4% H_2 environment resulted the diffusion of MnO into interfacial silica to form a Janus structure (designated as ***asy*-$MnSiO_3$@*h*-SiO_2**) having a circularly flattened patch of $MnSiO_3$ (42 ± 5 nm diameter, 21 ± 3 nm thickness). This was confirmed by transmission electron microscopy (TEM), scanning electron microscopy (SEM), STEM

[a] S. Kim, Dr. N. Kumari, J. Lim, Dr. S. Dubbu, Dr. A. Kumar, Prof. I. S. Lee
Center for Nanospace-confined Chemical Reactions (NCCR) and Department of Chemistry
Pohang University of Science and Technology (POSTECH)
Pohang 37673, South Korea
E-mail: amitkumar@postech.ac.kr (A.K.), insulee97@postech.ac.kr (I.S.L.)

[b] Prof. I. S. Lee
Institute for Convergence Research and Education in Advanced Technology (I-CREATE)
Yonsei University
Seoul 03722, South Korea

Supporting information for this article is given via a link at the end of the document.

10.1002/anie.202103165

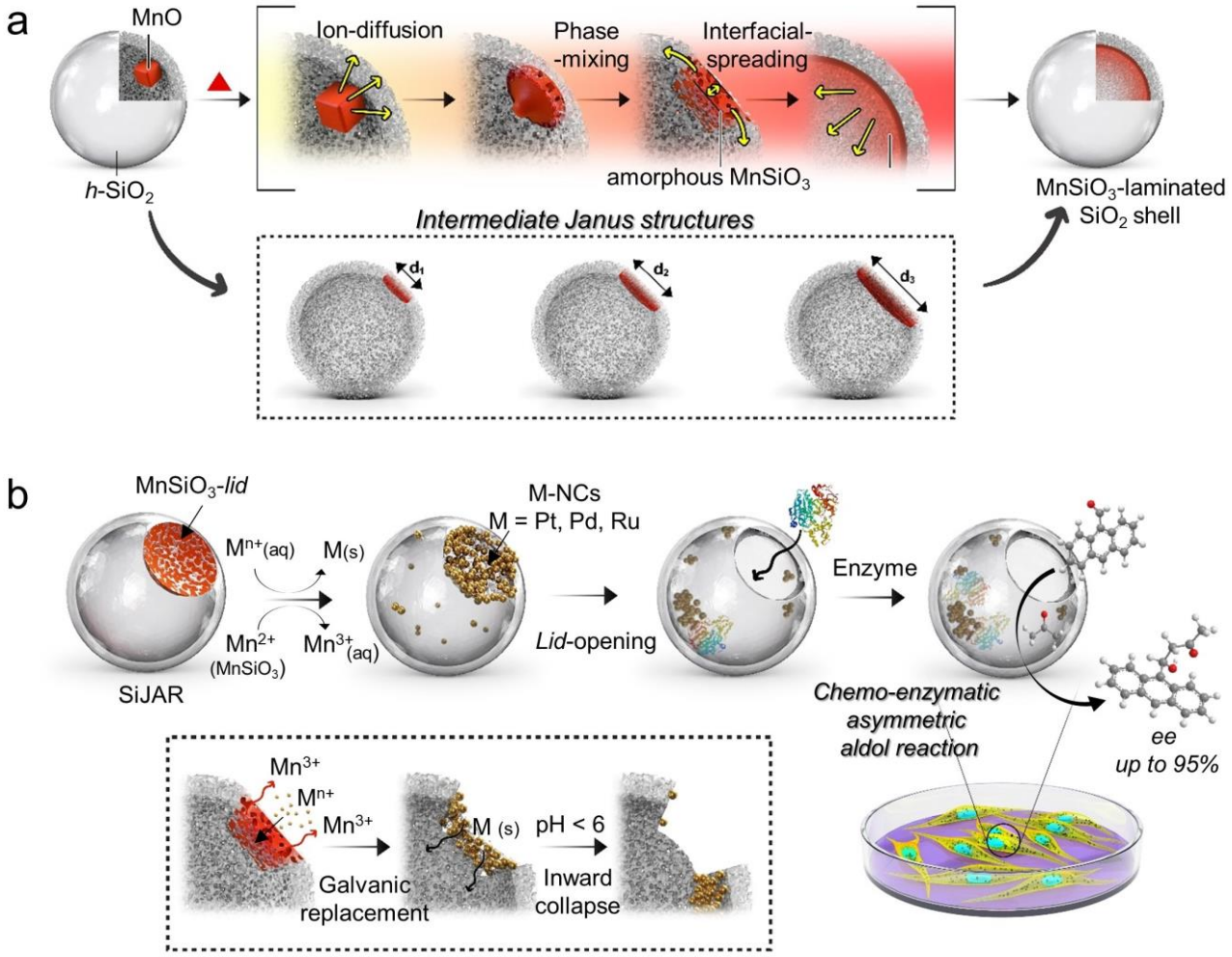

Figure 1. Schematic for: (a) solid-state thermal conversion process of **MnO@*h*-SiO₂** towards intermediate Janus ***asy*-MnSiO₃@*h*-SiO₂** (with controllable size of $MnSiO_3$ region) and symmetrical ***h*-MnSiO₃@SiO₂** structures. (b) Galvanic metal exchange reaction at the lid section of **SiJAR** followed by inward lid opening (detailed in the dotted box) and enzyme encapsulation inside **SiJAR** to conduct bioorthogonal chemo-enzymatic asymmetric aldol reaction.

and STEM-energy-dispersive X-ray spectroscopy (EDX)-based elemental mapping and line-profiling (Figure 2). At the MnO-diffusion site, the directional inclusion of Mn^{2+} into the selected interior silica network caused the predominantly inward volume expansion and left a segregated domain of amorphous $MnSiO_3$-phase [confirmed by X-ray diffraction analysis (XRD), Figure S1], which formed well-defined boundaries surrounded by unaffected segment of the *h*-SiO_2 (Figure 2). Such asymmetric morphological evolution is distinct from previously observed hollowing of tight MnO@SiO_2 core-shell, where Mn^{2+} moved into surrounding SiO_2 in an isotropic manner, forming a spherical hollow shell of $MnSiO_3$.[12] For additional mechanistic insights, we conducted reductive annealing of MnO@*h*-SiO_2 at different T_{ann} (600 ~ 900 °C) for 24 h (Figure S2). MnO didn't react until T_{ann} = 600 °C but started diffusing through the interfacial silica part at 700 °C and further transitioned to ***asy*-MnSiO₃@*h*-SiO₂** as the result of formation of amorphous $MnSiO_3$ phase at 750 ~ 800 °C. Interestingly, at higher temperature of T_{ann} > 850 °C, the $MnSiO_3$ domain appeared to spread out over through the interior surface of *h*-SiO_2 (time-course study in SI, Figure S3), changing the structure to a symmetrical *h*-SiO_2 shell with a thin $MnSiO_3$ laminate inside (***h*-MnSiO₃@SiO₂**). It can be reasoned by the viscous fluid-like movement of the $MnSiO_3$ phase, which assumed a liquid glass-like state at temperatures above its lowered glass transition temperature (T_g), and eventually coated the interior homogeneously with thin $MnSiO_3$ layer conformal-interfaced with outer SiO_2 phase (analyzed by EDX and XRD) as a result of thermodynamic lowering of interfacial surface energies of two immiscible solid-solid systems (Figure 2).[12a,18] Upon oxidative annealing at 800 °C in air, ***asy*-MnSiO₃@*h*-SiO₂** and ***h*-MnSiO₃@SiO₂** resulted the formation of tiny Mn_2O_3 NCs at the patch and all over the spherical shell, respectively, which confirmed their respective distributions of $MnSiO_3$ phase on silica shell (Figure S4).[12a] Alternatively, the annealing of a physical mixture of MnO NC and free *h*-SiO_2 produced sintered lumps along with empty silica shells, indicating the indispensable role of yolk-shell configuration (Figure S5). Unique composition and hollow *jar-like* interior of ***asy*-MnSiO₃@*h*-SiO₂** (hereafter designated as **SiJAR**s) allowed us to conduct their diversified post-synthetic transformations of the chemically responsive $MnSiO_3$ section which can function as a '*lid*' allowing on-demand mouth-opening and catalytic functionalization. Upon treatment

10.1002/anie.202103165

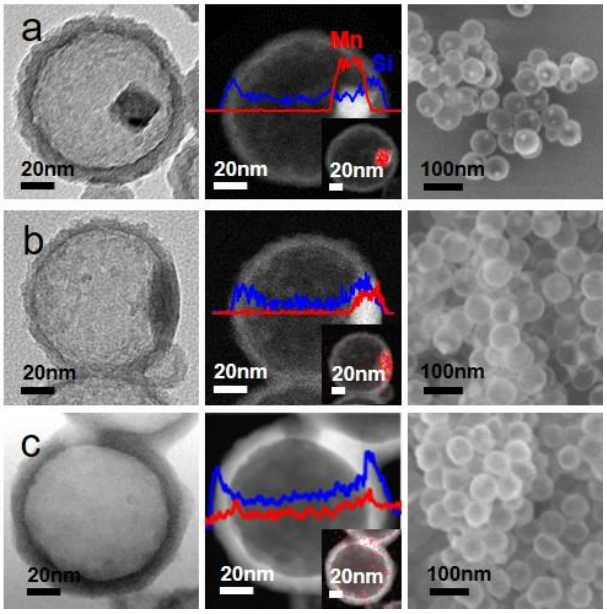

Figure 2. Characterization of ***asy*-MnSiO$_3$@*h*-SiO$_2$** and ***h*-MnSiO$_3$@SiO$_2$** thermally converted from MnO@*h*-SiO$_2$: HRTEM (left), STEM-EDS line profile (middle, inset : EDS mapping [Mn (red)] and SEM images (right) of MnO@*h*-SiO$_2$ (a) and annealed products at 800 °C (b, ***asy*-MnSiO$_3$@*h*-SiO$_2$**) and at 900 °C (c, ***h*-MnSiO$_3$@SiO$_2$**).

with acidic conditions (3 M HCl), a circular opening (44 ± 6 nm) in **SiJAR** was visualized due to pH-induced release of Mn^{2+} ions selectively from the $MnSiO_3$ *lid*-part, without affecting the remaining *jar*-like SiO_2 nanostructure (Figure 3a). Choosing the different size-ratios of MnO and *h*-SiO_2 components in the starting MnO@*h*-SiO_2 resulted different proportional sizes of the $MnSiO_3$-*lid*s, which in turn decided the different extent of mouth-opening on **SiJAR**s (Figure S6). Further, we subjected **SiJAR**s for galvanic replacement reactions in order to modify various catalytic metals by exploiting the reductive Mn^{2+} of $MnSiO_3$-*lid* (Figure 3b, S7).[13,16] Treatment of **SiJAR**s with aqueous Na_2PdCl_4 solution (15 mM) resulted gradual deposition of tiny Pd grains on to the *lid* section, resulting a negatively curved Pd-modified-*lid* on **SiJAR** (**Pd-*lid*@SiJAR**). This was in corroboration with the decrease in Mn elements and correlated increase in Pd contents, quantified by inductive coupled plasma (ICP) and EDX-analysis (Figure 3b, S7). The functionalization of **SiJARs** was further extended to other catalytic metals such as Pt and Ru (Figure S8). When **Pd-*lid*@SiJAR** was incubated in phosphate buffer solution (PBS, pH4.6) at 37℃, the perforated and fragile Pd-modified-lid (due to the residual Mn^{2+} dissolution) was gradually dissociated from the surface and internalized in to **SiJAR** body, guided by the negative curvature of the *lid*-section (Figure S9), resulting an open-mouth (opening size 44 ± 6 nm) structure accommodating ligand-free Pd NCs (**Pd@SiJAR**). Large mouth-opening and negatively curved hollow interior of **Pd@SiJAR** (4 wt% Pd, by ICP) was further utilized to encapsulate and stabilize the *Candida antractica* lipase A (Cal-A) [6-9 wt% by thermogravimetric analysis (TGA)] with Pd NCs (Figure 3c) a, generating a chemoenzymatic catalytic nanoreactor platform (**Cal-Pd@SiJAR**). The presence of Cal-A was further verified by Fourier Transform Infrared Spectroscopy (FTIR) and TGA (Figure 3d, S10). When SiJAR (devoid of any PdNCs) was used, enzyme loading efficiency was reduced (*ca.* 5 wt%) which indicated the crucial role of PdNCs in directing the enzyme encapsulation (Figure S11).

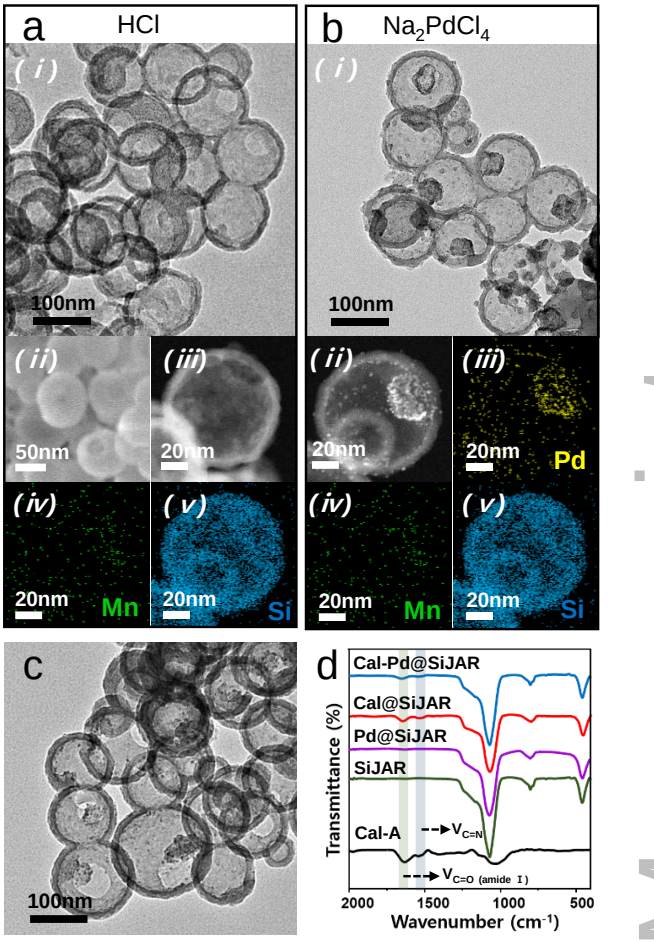

Figure 3. *Lid*-opening and catalyst functionalization with **SiJAR**: (a) TEM (*i*), SEM (*ii*) HADDF-STEM (*iii*) images and EDS elemental maps (*iv*, *v*) of HCl(*aq*) treated **SiJAR**s. (b) TEM (*i*), HADDF-STEM (*ii*) images and EDS elemental maps (*iii*-*v*) of **Pd-*lid*@SiJAR**s obtained after galvanic replacement in Pd precursor solution. (c) TEM image of **Cal-Pd@SiJAR**s. (d) FT-IR spectra of various samples.

To test the chemo-enzymatic catalytic performance of **Cal-Pd@SiJAR**, we chose direct aldol reaction (DAR), which is one of the most useful C-C bond forming tools for the synthesis of numerous active pharmaceuticals and synthons.[19, 25-26] Lipase is known to catalyze different reactions including DAR with broad substrate scope but often with poor enantioselectivities.[27] Moreover, direct application of free Lipase inside cell is not feasible due to delicate nature of the enzyme.The proximity of Pd NCs with Cal-A inside **SiJAR**, would stabilize a favorable transition state for high enantioselectivity.[20,23] In a test reaction, 4-nitrobenzaldehyde (0.1 mM) was reacted with acetone in the presence of **Cal-Pd@SiJAR** at r.t. for 30 h, affording the aldol product in quantitative yield (> 99% by ^{1}H NMR) and good enantiomeric excess (*ee* = *ca.* 95%) (Figure 4, S12-S14). Although, free Cal-A affected similar transformation, but could only afford poor enantiocontrol (*ee* < 11 %) (Figure 4, S15). Encapsulating only Cal-A inside **SiJAR** (**Cal@SiJAR**) resulted comparable *ee* as free enzyme but reaction rate was higher

10.1002/anie.202103165

WILEY-VCH

COMMUNICATION

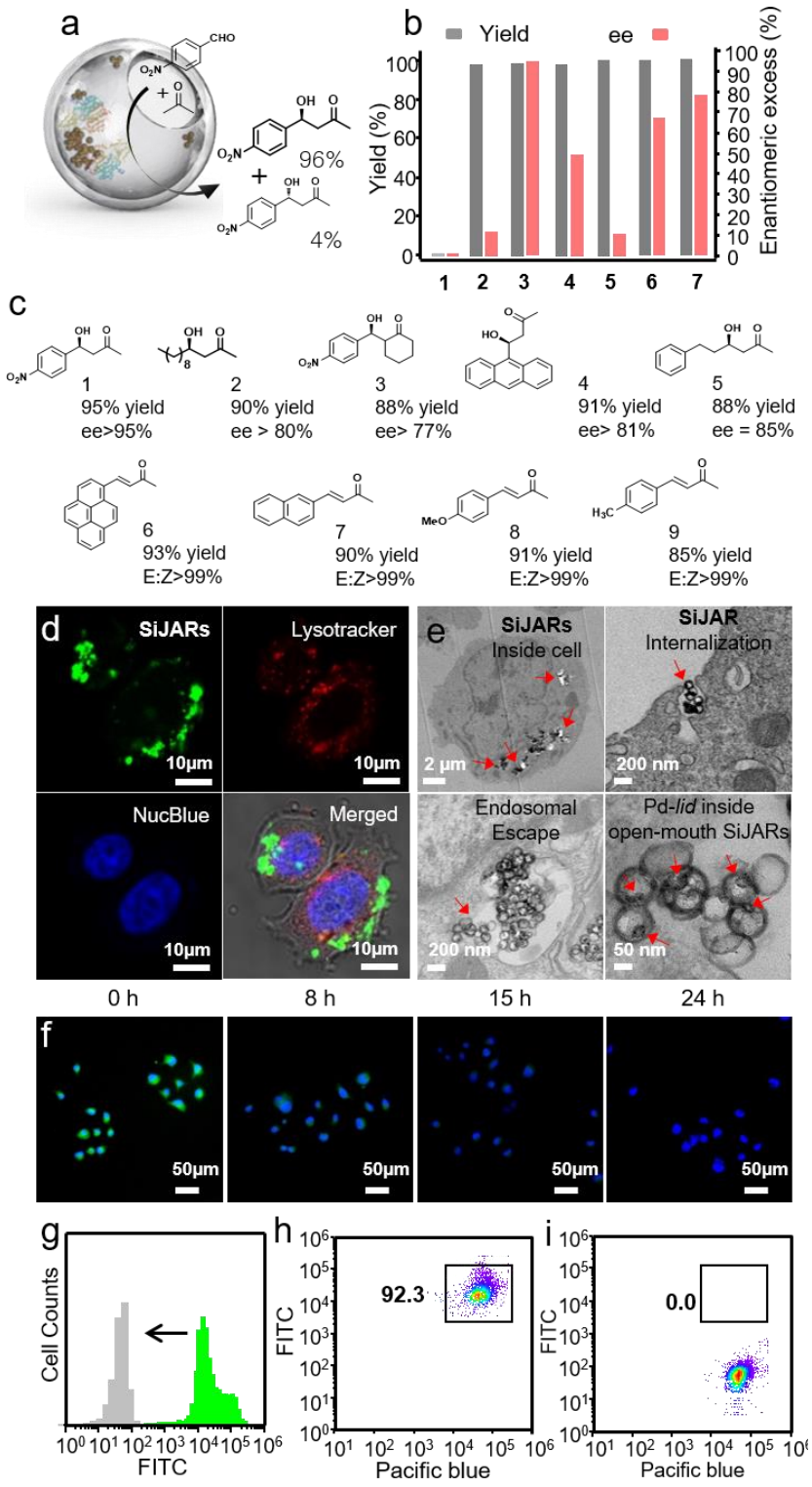

Figure 4. Catalytic test with **Cal-Pd@SiJAR**: (a) Schematic for asymmetric aldol reaction using **Cal-Pd@SiJAR**. (b) Yields and enantiomeric excess of the aldol reaction between 4-nitrobenzaldehyde and acetone using different catalysts: **1**- Pd@SiJAR, **2**- Cal A@SiJAR, **3**- Cal-Pd@SiJAR, **4**- CalA/Pd (physical mixture), **5**- Cal A, **6**- Cal A+Pd+SiO_2 (physical mixture), **7**- Cal-Glt-Pd-NH_2SiO_2. (c) Product yields and enantiomeric excess with different substrates using **Cal-Pd@SiJAR**. (d) CLSM images of MCF-7 cells after internalization with fluorescein modified **SiJARs** (green spots) and merged with Lysotracker and NucBlue staining. (e) TEM images of fixed and sectioned cells internalized with **Cal-Pd@SiJARs** (red arrows showing locations of the NPs). (f) Time-course fluorescence images (FITC filter) with NucBlue-staining showing decrease in green fluorescence as the result of catalytic reaction between fluorescent aldehyde and acetone forming the non-fluorescent aldol product. (g-i) Flow cytometry analysis showing a population of cells before (green) and after (gray) catalytic aldol reaction.

(Figure 4). Using only Pd NCs inside **SiJAR** (**Pd@SiJAR**) showed no reaction, affirming the indispensable role of Cal-A in carbonyl-group activation (Figure 4).[20] Nevertheless, a physical mixture of Cal-A and Pd NCs afforded improved enantioselectivity (*ee* = *ca.* 50%) which slightly improved upon adding silica nanospheres (*ee* = *ca.* 68%), indicating a favorable role of co-localized Pd NCs and Cal-A inside **SiJAR** towards chirality control (Figure 4, S16). During a reaction time-course using **Cal-Pd@SiJAR**, *ee* of product **1** was almost consistent over the time (Figure 4); also, a mixture of Pd NCs and chiral product **1** (without Cal-A) couldn't induce any aldol reaction, suggesting no chiral amplification mechanism through autocatalysis.[21] In addition, the treatment of **1** with Pd NCs for >30 h, didn't influence its enantiopurity through any possible [Pd]-induced C-H epimerization.[4a] In **Cal-Pd@SiJAR**, facile reactant/product transport and better transition state stabilization through the chemoenzymetic co-operative system located at negatively curved silica interior may be responsible for high reaction rates and enantioselectivities (Figure S17).[13a, 22, 27c, 28]

A range of aldehydes having different aromatic and aliphatic substitutions (Figure 4c), afforded good to excellent enantioselectivities of aldol products (**2**-**5**) (Figure S19-27). However, in some cases (**6**-**9**), α,β–unsaturated ketones were isolated as the final dehydrated products (Figure 4c). Notably, the catalyst could be recycled multiple times (up to 5 cycles) without any significant loss in the reactivity (< 10% loss in conversion yield) and enantioselectivity (*ee* = *ca.* 87% after 5th cycle) (Figure S28-30). A control catalyst (Cal-Glt-Pd-NH_2SiO_2) having PdNCs (*ca.* 1.4 nm) and CalA covalently linked (*ca.* 9 wt%) to the surface of colloidal aminated silica nanospheres (Figure S31) produced aldol product in quantitative yield but with 77% ee (Figure 4b), indicating the better enantio-control in the case of **Cal-Pd-SiJAR**. Next, we tested the feasibility of the catalyst's compartmentalized design under biorthogonal conditions. After incubation with human breast cancer cells (MCF-7 cells) **Cal-Pd@SiJAR** (< 400 μg/mL) remained highly biocompatible (cell viability *ca.* 85%, Figure S32), showing good cellular uptake (*ca.* 64%). The endocytosis, cytoplasmic localization and endosomal release of **SiJAR**s were affirmed by Bio-TEM and also imaged by high resolution confocal laser scanning microscopy (CLSM) (Figure 4d,e & Video S1). Next, we subjected **Cal-**

Pd@SiJAR for intracellular catalysis for aldol reaction between a fluorescent 9-antracenecarboxaldehyde with acetone to form a aldol product (**4**) with shifted fluorescence response (Figure S33). The intracellular aldol reaction (details in SI) was monitored by fluorescence microscopy and flow cytometry (Figure 4g-i). The initial strong green fluorescence inside the cells started fading within 8 h and disappeared after 24 h due to the formation of the aldol product **4** (Figure 4f). We isolated the aldol product **4** from the cell lysate and analyzed to show high *ee* (*ca.* 79%) (Figure S34). The absence of **Cal-Pd-SiJAR** or acetone showed consistent fluorescence signals until 24 h (Figure S35), validating that disappearance of fluorescence could only occur through the intracellular aldol reaction. After incubating with MCF-7 cells for 24 h, we retrieved the **Cal-Pd@SiJAR** through cell-lysis and affirmed their preserved nanostructure (by TEM) and catalytic performance using a standard colorimetric assay kit and aldol reaction (Figure S36-39). In comparison, Cal-Glt-Pd-NH_2SiO_2 did not induce any intracellular aldol reaction because of severe nanostructre deformation and deactivation (details in SI, Figure S40).[24]

In conclusion, we developed a solid-state NC-conversion strategy to selectively modify the controllable arc-section of *h*-SiO_2 with metal-silicate for installing a chemically responsive circular lid, which endowed noble metal decoration and size-controlled mouth-opening for the co-localization of catalytic metal NCs and enzymes inside **SiJARs**. As a key step, MnO-yolk acted as metal reservoir which docked and fused as Mn^{2+} into shell-section; the resulting *lid-on-jar* Janus shell was isolated as the intermediate structure before transitioning to symmetric biphasic-shell. These open-mouth chemo-enzymatic nanoreactors rendered high enantioselectivity for asymmetric aldol reaction through a cooperating transition state stabilization role of Pd and Cal-A co-supported on negatively curved silica-interior. Sub-100 nm sized **SiJARs** were highly biocompatible and easily internalized with living cells creating an organelle-like confined catalytic compartments inside cytoplasm. In future, these highly customizable hybrid chemoenzymatic nanodevices can be utilized for synthesizing active therapeutics and bioimging probes locally inside cells in order to develop next generation biomedical tools.

Acknowledgements

This work was supported by the Basic Science Research Program through the National Research Foundation of Korea (NRF) funded by the Ministry of Science, ICT & Future Planning (MSIP) (NRF-2016R1A3B1907559) (I.S.L.) and (NRF-2020R1I1A1A01071721) (A.K.).

Keywords: open-mouth nanoreactor • nanocrystal conversion chemistry • chemo-enzyme hybrid • nanocatalyst • enantioselective catalysis

[1] A. F. Mason, N. A. Yewdall, P. L. W. Welzen, J. Shao, M. Stevendaal, J. C. M. van Hest, D. S. Williams, L. K. E. A. Abdelmohsen, *ACS Cent. Sci.* **2019**, *5*, 1360–1365.

[2] a) K. Y. Lee, S. J. Park, K. A. Lee, S. H. Kim, H. Kim, Y. Meroz, L. Mahadevan, K. H. Jung, T. K. Ahn, K. K. Parker, K. Shin, *Nat. Biotechnol.* **2018**, *36*, 530–535; b) T. Einfalt, D. Witzigmann, C. Edlinger, S. Sieber, R. Goers, A. Najer, M. Spulber, O. Onaca-Fischer, J. Huwyler, C. G. Palivan, *Nat. Commun.* **2018**, *9*, 1127.

[3] a) M. Sancho-Albero, B. Rubio-Ruiz, A. M. Pérez-López, V. Sebastián, P. Martín-Duque, M. Arruebo, J. Santamaría, A. Unciti-Broceta, *Nat. Catal.* **2019**, *2*, 864–872; b) M. A. Miller, B. Askevold, H. Mikula, R. H. Kohler, D. Pirovich, R. Weissleder, *Nat. Commun.* **2017**, *8*, 15906; c) J. Clavadetscher, E. Indrigo, S. V. Chankeshwara, A. Lilienkampf, M. Bradley, *Angew. Chem. Int. Ed.* **2017**, *56*, 6864–6868; *Angew. Chem.* **2017,** *129,* 6968–6972.

[4] a) S. Dutta, N. Kumari, S. Dubbu, S. W. Jang, A. Kumar, H. Ohtsu, J. Kim, S. H. Cho, M. Kawano, I. S. Lee, *Angew. Chem. Int. Ed.* **2020**, *59*, 3416—3422; *Angew. Chem*. **2020**, *132,* 3444–3450; b) V. Smeets, W. Baaziz, O. Ersen, E. M. Gaigneaux, C. Boissière, C. Sanchez, D. P. Debecker, *Chem. Sci.* **2020**, *11*, 954–961; c) K. Engström, E. V. Johnston, O. Verho, K. P. J. Gustafson, M. Shakeri, C. W. Tai, J. E. Bäckvall, *Angew. Chem. Int. Ed.* **2013**, *52*, 14006–14010; *Angew. Chem.* **2013**, *125*, 14256–14260.

[5] a) Z. Du, C. Liu, H. Song, P. Scott, Z. Liu, J. Ren, X. Qu, *Chem.* **2020**, *6*, 1–13; b) J. J. Soldevila-Barreda, N. Metzler-Nolte, *Chem. Rev.* **2019**, *119*, 829–869; c) J. P. C. Coverdale, I. Romero-Canelón, C. Sanchez-Cano, G. J. Clarkson, A. Habtemariam, M. Wills, P. J. Sadler, *Nat. Chem.* **2018**, *10*, 347–354.

[6] a) A. Sousa-Castillo, J. R. Couceiro, M. Tomás-Gamasa, A. Mariño-López, F. López, W. Baaziz, O. Ersen, M. Comesaña-Hermo, J. L. Mascareñas, M. A. Correa-Duarte, *Nano Lett.* **2020**, *20*, 7068–7076; b) J. Lee, S. Dubbu, N. Kumari, A. Kumar, J. Lim, S. Kim, I. S. Lee, *Nano Lett.* **2020**, *20*, 6981–6988; c) W. Fang, J. Yang, J. Gong, N. Zheng, *Adv. Funct. Mater.* **2012**, *22*, 842–848.

[7] a) H. Che, S. Cao, J. C. M. van Hest, *J. Am. Chem. Soc.* **2018**, *140*, 5356–5359; b) P. Gobbo, A. J. Patil, M. Li, R. Harniman, W. H. Briscoe, S. Mann, *Nat. Mater.* **2018**, *17*, 1145–1153; c) L. -C. Lee, J. Lu, M. Weck, C. W. Jones, *ACS Catal.* **2016**, *6*, 784–787.

[8] a) G. Prieto, H. Tüysüz, N. Duyckaerts, J. Knossalla, G. -H. Wang, F. Schüth, *Chem. Rev.* **2016**, *116*, 14056–14119; b) Y. Li, J. Shi, *Adv. Mater.* **2014**, *26*, 3176–3205.

[9] C. Gao, F. Lyu, Y. Yin, *Chem. Rev.* **2020**, *121*, 834–881.

[10] a) S. Gao, Z. Wang, L. Ma, Y. Liu, J. Gao, Y. Jiang, *ACS Catal.* **2020**, *10*, 1375–1380; b) Q. Wang, X. Zhang, L. Huang, Z. Zhang, S. Dong, *Angew. Chem. Int. Ed.* **2017**, *56*, 16082–16085; *Angew. Chem.* **2017**, *129*, 16298–16301.

[11] a) Z. Teng, W. Li, Y. Tang, A. Elzatahry, G. Lu, D. Zhao, *Adv. Mater.* **2019**, *31*, 1707612; b) Y. Chen, H. –R. Chen, J. –L. Shi, *Acc. Chem. Res.* **2014**, *47*, 125–137.

[12] a) T. W. Kwon, K. -W. Jeon, S. Dutta, I. S. Lee, *Chem. Mater.* **2018**, *30*, 8070–8078; b) T. -L. Ha, J. G. Kim, S. M. Kim, I. S. Lee, *J. Am. Chem. Soc.* **2013**, *135*, 1378–1385.

[13] a) J. G. Kim, A. Kumar, S. J. Lee, J. H. Kim, D. -G. Lee, T. Kwon, S. H. Cho, I. S. Lee, *Chem. Mater.* **2017**, *29*, 7785–7793; b) S. M. Kim, M. Jeon, K. W. Kim, J. Park, I. S. Lee, *J. Am. Chem. Soc.* **2013**, *135*, 15714–15717.

[14] a) D. Yi, Q. Zhang, Y. Liu, J. Song, Y. Tang, F. Caruso, Y. Wang, *Angew. Chem. Int. Ed.* **2016**, *55*, 14733–14737; *Angew. Chem.* **2016**, *128*, 14953–14957; b) X. Li, L. Zhou, Y. Wei, A. M. El-Toni, F. Zhang, D. Zhao, *J. Am. Chem. Soc.* **2015**, *137*, 5903–5906; c) M. Alarcón-Correa, T.-C. Lee, P. Fischer, *Angew. Chem. Int. Ed.* **2015**, *54, 6730–6734*; *Angew. Chem.* **2015**, *127*, 6834–6838; d) D. A. Wilson, R. J. M. Nolte, J. C. M. van Hest, *J. Am. Chem. Soc.* **2012**, *134*, 9894–9897.

[15] a) J. Chen, F. Jiang, Y. Yin, *Acc. Chem. Res.* **2021**, *54*, 1168–1177; b) X. Wang, J. Liu, *ChemNanoMat* **2020**, *6*, 1437–1448; c) D. Wang, X. Wang, Z. Li, M. Chi, Y. Li, Y. Liu, Y. Yin, *ACS Nano* **2018**, *12*, 10949–10956.

[16] K. W. Kim, S. M. Kim, S. Choi, J. Kim, I. S. Lee, *ACS Nano* **2012**, *6*, 5122–5129.

[17] a) B. G. Cha, J. H. Jeong, J. Kim, *ACS Cent. Sci.* **2018**, *4*, 484–492; b) D. H. Han, H. -K. Na, W. H. Choi, J. H. Lee, Y. K. Kim, C. Won, S. -H. Lee, K. P. Kim, J. Kuret, D. -H. Min, M. J. Lee, *Nat. Commun.* **2014**, *5*, 5633.

[18] I. Avramov, T. Vassilev, I. Penkov, *J. Non-Cryst. Solids* **2005**, *351*, 472–476.

10.1002/anie.202103165

[19] B. List, *Chem. Rev.* **2007**, *107*, 5413–5415.

[20] C. Branneby, P. Carlqvist, A. Magnusson, K. Hult, T. Brinck, P. Berglund, *J. Am. Chem. Soc.* **2003**, *125*, 874–875.

[21] K. P. Bryliakov, *ACS Catal.* **2019**, *9*, 5418–5438.

[22] a) L. N. Pridgen, A. F. Abdel-Magid, I. Lantos, S. Shilcrat, D. S. Eggleston, *J. Org. Chem.* **1993**, *58*, 5107–5117; b) H. O. House, D. S. Crumrine, A. Y. Teranishi, H. D. Olmstead, *J. Am. Chem. Soc.* **1973**, *95*, 3310–3324.

[23] S. P. de Souza, R. A. C. Leão, J. F. Bassut, I. C.R. Leal, S. Wang, Q. Ding, Y. Li, F. L. –Y. Lam, R. O. M. A. de Souza, I. Itabaiana Jr, *Tetrahedron Lett.* **2017**, *58*, 4849-4854.

[24] J. G. Croissant, K. S. Butler, J. I. Zink, C. J. Brinker, *Nat. Rev. Mater.* **2020**, *5*, 886-909.

[25] B. M. Trost, C. S. Brindle, *Chem. Soc. Rev.* **2010**, *39*, 1600-1632.

[26] a) J. Paradowska, M. Pasternak, B. Gut, B. Gryzlo, J. Mlynarski, *J. Org. Chem.* **2012**, *77*, 173-187; b) X. Garrabou, J. A. Castillo, C. Guérard-Hélaine, T. Parella, J. Joglar, M. Lemaire, P. Clapés, *Angew. Chem. Int. Ed.* **2009**, *48*, 5521-5525; *Angew. Chem.* **2009**, *121*, 5629-5633.

[27] a) Z. S. Seddigi, M. S. Malik, S. A. Ahmed, A. O. Babalghith, A. Kamal, *Coord. Chem. Rev.* **2017**, *348*, 54-70; b) A. S. de Miranda, L. S. M. Miranda, R. O. M. A. de Souza, *Biotechnol. Adv.* **2015**, *33*, 372-393; c) E. Castillo, L. Casas-Godoy, G. Sandoval, *Biocatalysis* **2015**, *1*, 178-188.

[28] a) S. F. Motevalizadeh, M. Khoobi, A. Sadighi, M. Khalilvand-Sedagheh, M. Pazhouhandeh, A. Ramazani, M. A. Faramarzi, A. Shafiee, *J. Mol. Catal. B; Enzym*. **2015**, *120*, 75-83; b) A. Sadighi, S. F. Motevalizadeh, M. Hosseini, A. Ramazani, L. Gorgannezhad, H. Nadri, B. Deiham, M. R. Ganjali, A. Shafiee, M. A. Faramarzi, M. Khoobi, *Appl. Biochem. Biotechnol*. **2017**, *182*, 1371-1389.

10.1002/anie.202103165

WILEY-VCH

COMMUNICATION

Entry for the Table of Contents

Round bottom *jar*-like silica nanostructure (SiJAR) fitted with a Mn-silicate *lid* was fabricated through the highly controlled thermal solid-state conversion of a MnO nanocrystal at the inside of hollow SiO_2 shell. The *lid* aperture-opening created an open-mouth nanoreactor accommodating catalytic metal nanocrystals and enzymes, which performed asymmetric aldol reactions with high activity and enantioselectivity inside living cells.

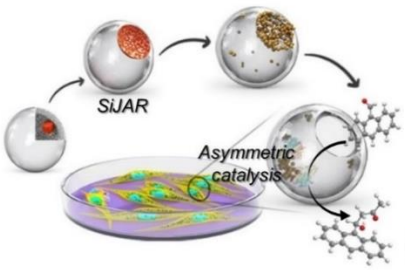

*Seonock Kim, Nitee Kumari, Jongwon Lim, Sateesh Dubbu, Amit Kumar * and In Su Lee **

Page No. – Page No.

Silica Jar-with-Lid as Chemo-Enzymatic Nano-Compartment for Enantioselective Synthesis inside Living Cells